

Differentiable Unsupervised Feature Selection

Yariv Aizenbud ^{1*} Ofir Lindenbaum ^{2*}

Yuval Kluger^{1†}

¹Yale University, USA; ² Bar-Ilan University, Israel;

[†]Corresponding author. E-mail: yuval.kluger@yale.edu

Address: 333 Cedar St, New Haven, CT 06510, USA

* These authors contributed equally.

Abstract

Anomalies (or outliers) are prevalent in real-world empirical observations and potentially mask important underlying structures. Accurate identification of anomalous samples is crucial for the success of downstream data analysis tasks. To automatically identify anomalies, we propose Probabilistic Robust AutoEncoder (PRAE). PRAE is designed to simultaneously remove outliers and identify a low-dimensional representation for the inlier samples. We first present the Robust AutoEncoder (RAE) intractable objective as a minimization problem for splitting the data to inlier samples from which a low dimensional representation is learned via an AutoEncoder (AE), and anomalous (outlier) samples that are excluded as they do not fit the low dimensional representation. RAE minimizes the autoencoder’s reconstruction error while incorporating as many samples as possible. This could be formulated via regularization by subtracting from the reconstruction term an ℓ_0 norm counting the number of selected samples. Unfortunately, this leads to an intractable combinatorial problem. Therefore, we propose two probabilistic relaxations of RAE, which are differentiable and alleviate the need for a combinatorial search. We prove that the solution to the PRAE problem is equivalent to the solution of RAE. We use synthetic data to show that PRAE can accurately remove outliers in a wide range of contamination frequencies. Finally, we demonstrate that using PRAE for anomaly detection leads to state-of-the-art results on various benchmark datasets.

1 Introduction

Unsupervised anomaly detection is a fundamental problem in data mining and machine learning. The goal is to identify unusual measurements in unlabeled datasets. Identifying anomalous samples is essential for empirical science in various fields, such as biology [1], geophysics [2, 3], engineering, and cyber-security [4]. Anomalies (also called outliers) are samples that significantly deviate from the “normal” (often majority) observations. A critical challenge is defining such normality and automatically identifying all abnormal measurements.

One line of methods for anomaly detection relies on the density of the data. By estimating the data density, anomalies could be identified as samples drawn from the low probability density regions. Density-based models include Local Outlier Factor (LOF) [5], or some of its variants such as [6, 7, 8]. More recent probabilistic approaches include [9, 10]. Other schemes, such as [11, 12, 13, 14] rely on distances between samples to identify anomalies; the basic assumption is that normal points have dense neighborhoods while outliers are far from their neighbors.

High dimensional measurements may often be described by a low dimensional subspace or manifold [15, 16, 17]. By assuming that the normal samples lie near a low dimensional latent manifold, while outliers are diverse and do not follow the same manifold structure, the anomalies could be detected via a dimensionality reduction method, such as Principal Component Analysis (PCA) [18], or deep Autoencoders (AE) [19]. Robust PCA schemes [20] seek for a low dimensional linear subspace that fits “best” the inliers. These models can identify anomalies and learn a reduced sup-space simultaneously; however, they are restricted to linear transformations. To overcome this limitation, several authors have proposed to use sparse AEs [21, 22]. Ensemble Autoencodes [21] use multiple AEs trained with different subsets of the observations and evaluate the reconstruction error to identify outliers. In [22] the authors propose an $\ell_{2,1}$ regularized reconstruction loss with an additional constrain to split the data matrix into two matrices that approximately represent inliers and outliers. Other generative or semi-supervised deep neural networks for detecting anomalies were proposed in [23, 24, 25].

In this work, we propose a novel Probabilistic Robust autoencoder (PRAE) for anomaly detection. PRAE can simultaneously remove outliers and learn a low-dimensional representation of the inlier samples. First, we describe the robust autoencoding (robust-AE) problem by incorporating an ℓ_0 term penalizing the number of observations included in the AE’s reconstruction loss. Then, we propose two probabilistic relaxations for robust-AE and demonstrate that they could be effectively trained using standard optimization tools such as stochastic gradient descent. We show theoretically that the solution of the probabilistic relaxation is equivalent to the solution to the robust-AE problem. Finally, we demonstrate using extensive simulations that probabilistic robust-AE (PRAE) outperforms leading anomaly detection methods in multiple settings.

2 Background

2.1 Notation

Throughout the paper we denote vectors using **bold** lowercase letters such as \mathbf{x} . Scalars are denoted by lower case letters such as y . The n^{th} vector-valued observation is denoted as \mathbf{x}_n while $x[d]$ represents the d^{th} feature (or entry) of the vector \mathbf{x} . Matrices are denoted by **bold** uppercase letters \mathbf{X} . The ℓ_p norm of \mathbf{x} is denoted by $\|\mathbf{x}\|_p$.

2.2 Autoencoder

The AE is a multilayer neural network designed for dimensionality reduction. It comprises an encoder and decoder, which are typically symmetric and are trained jointly to minimize the reconstruction error of the data. The number of neurons in the latent space (the hidden layer between the encoder and decoder) controls the dimension of the reduced representation of the data. It has been shown that the reduced representation of a linear AE spans the same subspace as the principal components of the data [26].

Given samples $X = \{\mathbf{x}_1, \dots, \mathbf{x}_N\}$, where $\mathbf{x}_i \in \mathbb{R}^D$, the AE learns the reduced representation by minimizing the following reconstruction loss

$$\frac{1}{N} \sum_i \left\| \mathbf{x}_i - \hat{\mathbf{x}}_i \right\|_2^2, \quad (1)$$

where the reconstructed vector $\hat{\mathbf{x}}_i$ is obtained as the output of the encoder $\rho()$ and decoder $\psi()$, i.e. $\hat{\mathbf{x}}_i = \psi(\rho(\mathbf{x}_i))$. The encoder-decoder pair are defined using a multi-layer neural network;

this can be described using the following equations:

$$\begin{aligned}\boldsymbol{\rho}_\ell(\mathbf{x}) &= \boldsymbol{\sigma}(\mathbf{W}_{\ell-1}^\rho \boldsymbol{\rho}_{\ell-1}(\mathbf{x}) + \mathbf{b}_{\ell-1}^\rho), \ell = 1, \dots, L, \\ \boldsymbol{\psi}_\ell(\mathbf{z}) &= \boldsymbol{\sigma}(\mathbf{W}_{\ell-1}^\psi \boldsymbol{\psi}_{\ell-1}(\mathbf{z}) + \mathbf{b}_{\ell-1}^\psi), \ell = 1, \dots, L,\end{aligned}$$

where $\boldsymbol{\rho}^{(0)}(\mathbf{x}) = \mathbf{x}$ and $\boldsymbol{\psi}_0(\mathbf{z}) = \mathbf{z} = \boldsymbol{\rho}_L(\mathbf{x})$. The weights \mathbf{W}_ℓ^ρ , \mathbf{W}_ℓ^ψ and biases \mathbf{b}_ℓ^ρ , \mathbf{b}_ℓ^ψ at each layer ℓ are learnt by applying stochastic gradient descent to the reconstruction loss. The operator $\boldsymbol{\sigma}$ is a nonlinear activation function applied in an element-wise fashion.

3 Method

3.1 Robust Autoencoder

Given samples $\mathbf{X} = \{\mathbf{x}_1, \dots, \mathbf{x}_N\}$, where $\mathbf{x}_i \in \mathbb{R}^D$, we model the data by $\mathbf{X} = \mathbf{X}_{in} \cup \mathbf{X}_{out}$, where \mathbf{X}_{in} are inliers and \mathbf{X}_{out} are outliers. We assume that \mathbf{X}_{in} can be approximated by some low dimensional structure. Our goal is to identify the inliers and outliers. We propose to use a regularized AE that simultaneously learns a low dimensional representation of the data and identifies the outliers. We define an indicator vector $\mathbf{b} \in \{0, 1\}^N$ whose value i indicates if the sample \mathbf{x}_i is an inlier ($b[i] = 1$) or an outlier ($b[i] = 0$). To learn the parameters of the encoder-decoder pair ($\boldsymbol{\rho}()$ and $\boldsymbol{\psi}()$) while simultaneously identifying the inliers and outliers, we propose the following robust deterministic AE loss

$$L_d(\boldsymbol{\psi}, \boldsymbol{\rho}, \mathbf{b}) = \sum_i b[i] \left\| \mathbf{x}_i - \hat{\mathbf{x}}_i \right\|_2^2 - \lambda \|\mathbf{b}\|_0, \quad (2)$$

where $\hat{\mathbf{x}}_i = \boldsymbol{\psi}(\boldsymbol{\rho}(\mathbf{x}_i))$. The leading term in Eq. (2) is a standard AE reconstruction term computed only for samples with $b[i] = 1$. The ℓ_0 norm in Eq. (2) counts the number of samples that are included in the reconstruction error; these samples are tagged as ‘‘inliers’’. By balancing the reconstruction error and the ℓ_0 penalty, the hyper-parameter λ controls the cost associated with the number of samples used by the AE. A large value of λ will force the model to include more samples. On the other hand, a small λ would lead to a sparser solution with fewer samples included by the model. If \mathbf{X}_{in} lie near a low dimensional manifold, we assume that the encoder-decoder pair can lead to a good approximation of the inliers, that is $\hat{\mathbf{x}}_i \approx \mathbf{x}_i$ for $\mathbf{x}_i \in \mathbf{X}_{in}$. On the other hand, if outliers do not lie near the low dimensional manifold, we expect $\|\mathbf{x}_i - \hat{\mathbf{x}}_i\|_2^2$ to be large. Unfortunately, due to the ℓ_0 norm in Eq. (2) the problem becomes intractable even for a small number of samples. To overcome this limitation, following [27, 28, 29], we propose to replace the deterministic search over the values of the indicator vector \mathbf{b} with a probabilistic counterpart.

3.2 Probabilistic Autoencoder

We are now ready to present our probabilistic formulation for a sparse AE. Towards this goal, we multiply the samples by stochastic gates that relax the binary nature of the indicator vector \mathbf{b} . The gates are differentiable and are purposed to select a subset of samples on which the AE reconstruction error is minimized. Following [27, 30, 31] we parameterize a stochastic gate (STG) using mean shifted truncated Gaussian distribution. Specifically, we denote the STG random vector as $\mathbf{z} \in [0, 1]^N$, parametrized by $\boldsymbol{\mu} \in \mathbb{R}^N$. Each vector entry is defined as

$$z[i] = \max(0, \min(1, \mu[i] + \epsilon[i])), \quad (3)$$

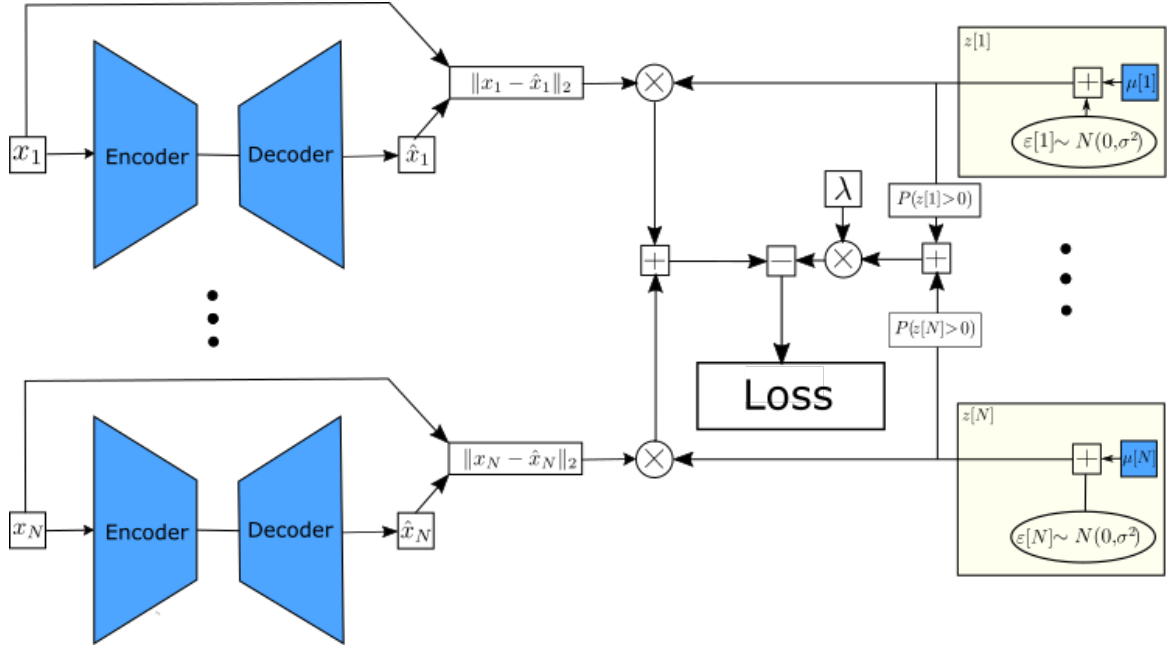


Figure 1: A schematic of the PRAE- ℓ_0 algorithm (see Eq. (4)). The x_i s (on the left) are the input samples. For any choice of encoder, decoder, and μ (all in blue), a score is computed (on the right). We optimize over the “blue” variables (the encoder, decoder, and μ that result in the lowest score). The resulting μ determines the outliers in the data.

where $\epsilon[i]$ is drawn from $\mathcal{N}(0, \sigma^2)$, σ is fixed throughout training, and $\mu[i]$ is a trainable parameter which controls the distribution of the random variable $z[i]$.

We can now incorporate the STGs into our proposed probabilistic AE loss. Formally, using the reconstruction loss of (1), a probabilistic AE loss can be described using one of the following terms

$$L_{p_0}(\psi, \rho, \mu) = \mathbb{E} \left(\sum_i z[i] \left\| \mathbf{x}_i - \hat{\mathbf{x}}_i \right\|_2^2 - \lambda \| \mathbf{z} \|_0 \right), \quad (4)$$

$$L_{p_1}(\psi, \rho, \mu) = \mathbb{E} \left(\sum_i z[i] \left\| \mathbf{x}_i - \hat{\mathbf{x}}_i \right\|_2^2 - \lambda \| \mathbf{z} \|_1 \right), \quad (5)$$

where, λ is a regularization parameter that controls the cost associated with the number of samples included by the AE. To minimize the new loss functions (4) or (5), we propose the following strategy. Given some initial guess for the encoder, decoder, parameterized via the weights of ψ and ρ , we draw realizations for the random vector \mathbf{z} and compute the loss value. We note that the regularization terms $\mathbb{E}(\| \mathbf{z} \|_0) = \sum P(z[i] > 0)$ and $\mathbb{E}(\| \mathbf{z} \|_1) = \sum \mathbb{E}(z[i])$ are parametric, and the expected value of the left term in (4) and (4) is approximated using Monte Carlo sampling. Then, we differentiate the loss using Stochastic Gradient Descent to update the weights in ψ and ρ , and the vector μ . A schematic illustration of this procedure is presented in Figure 1. A procedure for tuning the regularization parameter λ is discussed in Section 6.2.

4 Related Work

The problem of anomaly detection has been previously addressed using AEs. A straightforward solution is to train a standard AE and use the reconstruction error of each sample to quantify

if it is normal or anomalous [32]. Since this approach does not include regularization, the AE may overfit and lead to small reconstruction loss on outliers. To solve this limitation, in [21] the authors propose an ensemble of AEs for anomaly detection. The idea is to train many AEs, each pruned by randomly subsampling the learned connectivities. Then, an aggregated prediction of the ensemble is used for identifying the anomalies. One disadvantage of this approach is that it requires extensive computational and memory costs since it involves training hundreds of AEs. Furthermore, the proposed scheme outperforms the ensemble of AEs on several benchmark datasets.

Perhaps the most related to method to our work is [22]. In [22], the authors proposed the following regularized AE objective

$$\begin{aligned} & \| \mathbf{L}_D - \psi(\boldsymbol{\rho}(\mathbf{L}_D)) \|_2 + \lambda \| \mathbf{S} \|_{2,1} \\ & \text{s.t. } \mathbf{X} - \mathbf{L}_D - \mathbf{S} = 0. \end{aligned}$$

This model aims to split the data \mathbf{X} into two parts, \mathbf{L}_D and \mathbf{S} while minimizing the reconstruction error on \mathbf{L}_D . The regularization in the form of an $\ell_{2,1}$ norm is designed to sparsify the rows (samples) or columns (features) of \mathbf{S} . To minimize the objective with the additional constrain, they use the Alternating Direction Method of Multiplies (ADMM) [33] with an element-wise projection approach to enforce the constrain. This method differs from our approach significantly since the regularization relies on the $\ell_{2,1}$ norm applied to \mathbf{S} . This leads to shrinkage of values, and therefore \mathbf{S} is not guaranteed to reflect actual samples from \mathbf{X} . Furthermore, it relies on a different optimization scheme and is not amenable to parallelization through small batch training (due to the additional constrain).

5 Analysis

In this section, we justify the use of our proposed probabilistic AE (see Section 3.2) to solve the problem of sparse AEs (see Section 3.1). Since the latter is not differentiable while the first is, our goal is to show that both minimization problems lead to the same solution.

First, to avoid divergence of the values of $\boldsymbol{\mu}$ in the theoretical analysis, we bound the values of $\boldsymbol{\mu}$ by

$$-M \leq \boldsymbol{\mu}[i] \leq M, \quad (6)$$

for some large number M .

For any vector $\mathbf{b} \in \{0, 1\}^N$, we define $\boldsymbol{\mu}_b$, such that $\boldsymbol{\mu}_b[i] = -M$ if $\mathbf{b}[i] = 0$, and $\boldsymbol{\mu}_b[i] = M$ if $\mathbf{b}[i] = 1$ for $i = 1 \dots N$. For any $\boldsymbol{\mu}$ we define \mathbf{b}_μ such that $\mathbf{b}_\mu[i] = \text{sign}(\boldsymbol{\mu}[i])$.

We now turn our attention to show that the deterministic optimization problem (2) (which is not differentiable) is equivalent to our probabilistic optimization (5) in the following sense

Theorem 5.1. *For any dataset \mathbf{X} , denote by $(\boldsymbol{\psi}_d, \boldsymbol{\rho}_d, \mathbf{b}_d)$ the minimizer of (2) and by $(\boldsymbol{\psi}_p, \boldsymbol{\rho}_p, \boldsymbol{\mu}_p)$ the minimizer of (5). Assume that the minimizer of (2) is unique and that*

$$\min_{(\boldsymbol{\psi}, \boldsymbol{\rho}, \mathbf{b}) \neq (\boldsymbol{\psi}_d, \boldsymbol{\rho}_d, \mathbf{b}_d)} L_d(\boldsymbol{\psi}, \boldsymbol{\rho}, \mathbf{b}) \geq L_d(\boldsymbol{\psi}_d, \boldsymbol{\rho}_d, \mathbf{b}_d) + \varepsilon_0 \quad (7)$$

for some $\varepsilon_0 > 0$. Then for a sufficiently large $M > 0$ (see (6)), $(\boldsymbol{\psi}_d, \boldsymbol{\rho}_d) = (\boldsymbol{\psi}_p, \boldsymbol{\rho}_p)$, and for any $i = 1, \dots, L$, $b[i] = 1$ if $\mu[i] > 0$ and $b[i] = 0$ otherwise.

Or in other words if the minimizer of (2) is unique then, the encoder, decoder that minimize (2) and (5) are equivalent. Moreover, the samples included by the two models (indicated by \mathbf{b} and \mathbf{z}) are the same.

Proof. The proof construction is comprised of three arguments. The final argument relies on the first two and concludes the proof.

Argument 1: For any triplet $(\psi_d, \rho_d, \mathbf{b})$ the deterministic loss L_d can be approximated by the probabilistic loss L_{p_1} . Namely, for any $\varepsilon, \delta > 0$ there is a value of $M > 0$ such that

$$|L_d(\psi_d, \rho_d, \mathbf{b}_d) - L_{p_1}(\psi_d, \rho_d, \mu_b)| \leq \varepsilon,$$

with probability $1 - \delta$.

To prove this argument, we first compute the expectation $E(z)$ by definition using (3), we get:

$$\begin{aligned} E(z) &= \mu - \frac{1}{\sqrt{2\pi}} \int_{-\infty}^0 te^{-\frac{(t-\mu)^2}{2\sigma^2}} dt \\ &\quad - \frac{1}{\sqrt{2\pi}} \int_1^\infty te^{-\frac{(t-\mu)^2}{2\sigma^2}} dt + \frac{1}{\sqrt{2\pi}} \int_1^\infty e^{-\frac{(t-\mu)^2}{2\sigma^2}} dt, \end{aligned}$$

computing the integrals with the appropriate limits leads to:

$$\begin{aligned} E(z) &= \frac{\sigma}{\sqrt{2\pi}} (e^{-\frac{\mu^2}{2\sigma^2}} - e^{-\frac{(1-\mu)^2}{2\sigma^2}}) + (\mu - 1) * \Phi\left(\frac{1-\mu}{\sigma}\right) \\ &\quad - \mu * \Phi\left(-\frac{\mu}{\sigma}\right) + 1, \end{aligned}$$

where $\Phi()$ is the CDF of the standard normal distribution.

Since $\lim_{\mu \rightarrow \infty} E(z) = 1$, and $\lim_{\mu \rightarrow -\infty} E(z) = 0$, than, for any $\varepsilon > 0$, there is a sufficiently large M , such that

$$\left| \lambda \sum_i \mathbb{E}(z[i]) - \lambda \|\mathbf{b}\|_0 \right| < \varepsilon/2. \quad (8)$$

From the definition of z we also know that for $\mu > 1$, $P(z \neq 1) = \Phi(\frac{1-\mu}{\sigma})$, and thus $\lim_{\mu \rightarrow \infty} P(z = 1) = 1$. Similarly $\lim_{\mu \rightarrow -\infty} P(z = 0) = 1$. Thus, for any δ there is M large enough, such that

$$\left| \sum_i z[i] \|\mathbf{x}_i - \hat{\mathbf{x}}_i\|_2^2 - \sum_i b[i] \|\mathbf{x}_i - \hat{\mathbf{x}}_i\|_2^2 \right| < \varepsilon/2, \quad (9)$$

with probability $1 - \delta$.

Combining (8) and (9), we have that for any $\delta > 0$, there is a value of M such that

$$|L_d(\psi_d, \rho_d, b_d) - L_{p_1}(\psi_d, \rho_d, \mu_b)| \leq \varepsilon,$$

with probability $1 - \delta$. This concludes the proof of Argument 1.

Argument 2: For any AE (ψ, ρ) , the minimum $\min_{\mu} L_{p_1}(\psi, \rho, \mu)$ is achieved when $\mu[i]$ equals to either M or $-M$ for all i .

Assume by contradiction that the minimum of L_{p_1} is achieved at a point where for some k , $\mu[k]$ is not either M or $-M$. If

$$\left\| \mathbf{x}_i - \hat{\mathbf{x}}_i \right\|_2^2 \geq \lambda,$$

than for $\hat{\mu}$ such that $\hat{\mu}[i] = \mu[i]$ for all $i \neq k$ and $\hat{\mu}[k] = -M$ we have that

$$L_{p_1}(\psi, \rho, \hat{\mu}) \leq L_{p_1}(\psi, \rho, \mu),$$

which contradicts the minimality of $L_{p_1}(\boldsymbol{\psi}, \boldsymbol{\rho}, \boldsymbol{\mu})$. In case

$$\left\| \mathbf{x}_i - \widehat{\mathbf{x}}_i \right\|_2^2 \leq \lambda$$

a similar argument will lead to a contradiction as well.

Argument 3: Assume by contradiction that the minimizer of (2) is not equivalent to the minimizer of (5), i.e.

$$(\boldsymbol{\psi}_d, \boldsymbol{\rho}_d, \boldsymbol{\mu}_{b_d}) \neq (\boldsymbol{\psi}_p, \boldsymbol{\rho}_p, \boldsymbol{\mu}_p). \quad (10)$$

From Argument 2 we have that $\mu_p[i] = M$ or $-M$ for all i . From Argument 1 we have that

$$\|L_d(\boldsymbol{\psi}_p, \boldsymbol{\rho}_p, \mathbf{b}_{\mu_p}) - L_{p_1}(\boldsymbol{\psi}_p, \boldsymbol{\rho}_p, \mu_p)\| \leq \varepsilon, \quad (11)$$

and,

$$\|L_d(\boldsymbol{\psi}_d, \boldsymbol{\rho}_d, \mathbf{b}_d) - L_{p_1}(\boldsymbol{\psi}_d, \boldsymbol{\rho}_d, \mu_{b_d})\| \leq \varepsilon. \quad (12)$$

Since $\boldsymbol{\psi}_p, \boldsymbol{\rho}_p, \boldsymbol{\mu}_p$ is the minimizer of L_{p_1} , we have from (11) and (12) that

$$L_d(\boldsymbol{\psi}_d, \boldsymbol{\rho}_d, \mathbf{b}_d) \geq L_d(\boldsymbol{\psi}_p, \boldsymbol{\rho}_p, \mathbf{b}_{\mu_p}) - 2\varepsilon. \quad (13)$$

From Eq. (10) and the assumption of the theorem in Eq. (7), we have that

$$\|L_d(\boldsymbol{\psi}_p, \boldsymbol{\rho}_p, \mathbf{b}_{\mu_p}) - L_d(\boldsymbol{\psi}_d, \boldsymbol{\rho}_d, \mathbf{b}_d)\| \geq \varepsilon_0. \quad (14)$$

For $2\varepsilon < \varepsilon_0$, Eq. (14) contradicts Eq. (13). \square

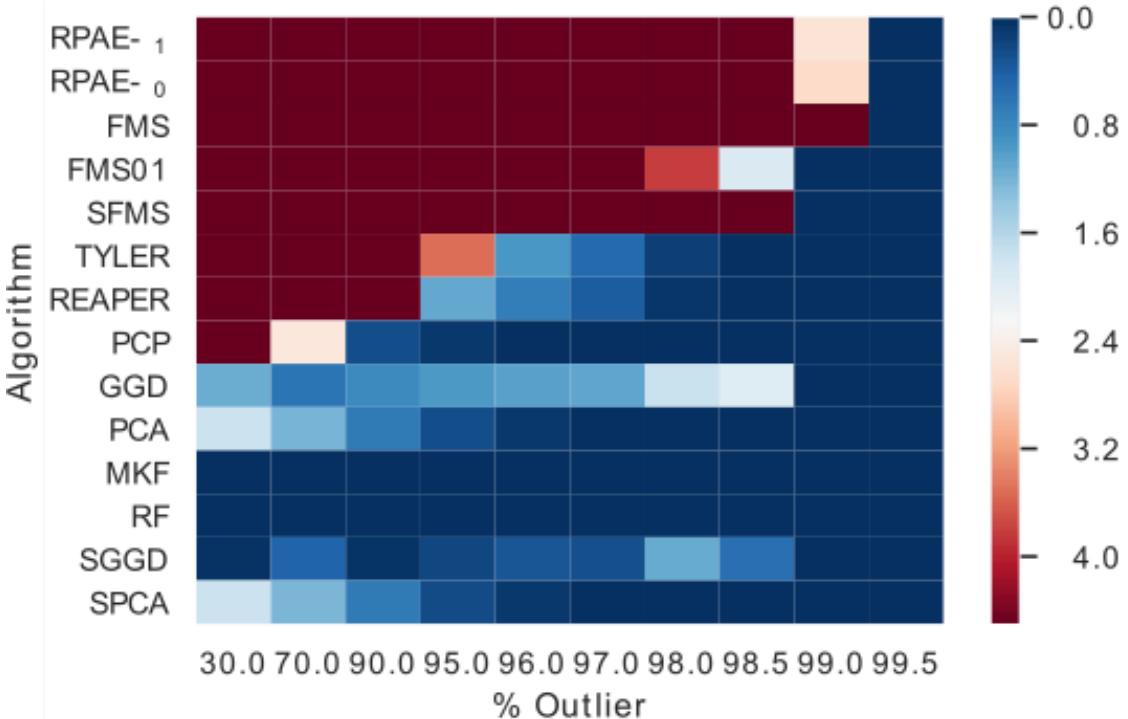


Figure 2: Comparing PRAE to several Robust Subspace Recovery (RSR) algorithms. The y-axis represents the different algorithms, and the x-axis represents different percentiles of outliers. Each box is colored according to the mean over 10 runs of the log of the angle between the recovered subspace and the ground truth.

6 Experiments

The following section describes the experimental evaluation performed to assess the proposed method.

6.1 Linear embedding

First, we test the performance of the proposed algorithms in the linear setting. While this regime has fewer applications, it is well studied, and it is easier to analyze and compare different methods.

We note that in the linear regime, the outlier detection problem is strongly related to the Robust Subspace Recovery problem (RSR). Thus, this section focuses on comparing our proposed scheme to baseline methods designed to solve the RSR problem. The RSR problem involves finding a low-dimensional (linear) subspace in a corrupted, potentially high-dimensional data set. For a complete overview of RSR, we refer the reader to [20].

In this section we conduct the following experiment, repeated from [20]. We generate $N = 10000$ data points in \mathbb{R}^{200} in the following way: first we randomly generate \mathbf{X}_{in}^{low} , a set of N_{in} random points in \mathbb{R}^{10} . Next we generate a random linear transformation $\mathbf{T} \in \mathbb{R}^{200 \times 10}$, and set $\mathbf{X}_{in}^{high} = \mathbf{T}\mathbf{X}_{in}^{low} + \text{noise}$, where $\text{noise} \sim N(0, 10^{-8})$. Finally, we generate \mathbf{X}_{out} as random points in \mathbb{R}^{200} , and define the data set $\mathbf{X} = \mathbf{X}_{in}^{high} \cup \mathbf{X}_{out}$. The task is to recover \mathbf{T} and \mathbf{X}_{in} given the data \mathbf{X} . The accuracy is measured by the log of the angle between the recovered \mathbf{T} and the correct \mathbf{T} . Each experiment was performed 10 times, and the final outcome is the average of the 10 runs.

The result of the comparison to other algorithms under different percentile of outliers appears in Figure 2. The two algorithms of this paper are compared to the following: fast median subspace (FMS) [34], Tyler’s M-estimator (TYLER) [35], REAPER [36], the augmented Lagrange multiplier method (PCP)[37], geodesic gradient descent (GGD) [38], and principal component analysis (PCA). In the overview, paper [20], more algorithms were compared. We chose the ones that performed best.

While our approach is not explicitly designed for the RSR (linear) problem, it is easy to see that our algorithms perform similarly to the state-of-the-art methods for RSR. Even for 99% outliers, in 7 out of 10 runs, our algorithms found exactly all the inliers. We note that since our approach is not designed for RSR and focused on the more general non-linear setting, FMS outperforms it and requires a shorter training time. Nonetheless, we argue that this experiment highlights that our model is relatively robust to the number of outliers.

6.2 Hyper-parameter Tuning

The proposed algorithm relies on a regularization term, namely the ℓ_0 or ℓ_1 norm (see (4) and (5)). An important practical consideration is the choice of regularization parameter λ . In this section, we empirically study the effect of this regularization parameter. Then, we propose two unsupervised schemes for tuning the regularization parameter. Finally, we use synthetic data to demonstrate our estimated regularization parameters leads to correct identification of all inliers and removal of all outliers.

Here, we focus on the linear data model described in section 6.1, but with $N = 200$, $\mathbf{X}_{in}^{low} \in \mathbb{R}^{150 \times 2}$, and $\mathbf{T} \in \mathbb{R}^{100 \times 2}$. We generate data from this model and run PRAE- ℓ_0 , and PRAE- ℓ_1 for various values of λ in the range $[0.1, 10]$. We run each model 20 time and record the average F1-score of each model. Here, we compute the F1-score using the precision and recall, which are defined based on outlier identification. Specifically, we define an outlier \mathbf{x}_i as a

sample such that after training $z[i] < \text{thresh}$, and an inlier otherwise. Here, $z[i]$ is computed based on Eq. 3 but without the injected Gaussian noise. We set thresh to 0.1 although other values within $(0, 1)$ lead to similar results.

In both of our proposed loss functions (see (4) and (4)) λ balances between the number of sample included by the model and the reconstruction loss. For a very large λ , we expect the model to include all samples since the regularization term would be larger than the reconstruction of \mathbf{x}_i (for inliers and outliers). On the other hand, if $\lambda = 0$ all samples should be excluded by the model. For small values of $\lambda > 0$, we expect the model to include the inliers (since we can obtain zero reconstruction loss) and exclude the outliers. Based on the linear model experiment (described above), we observe a "phase transition" in the behavior of PRAE as a function of λ . Namely, as evident in the top panel of Figure 3 for small values of λ , PRAE removes all outliers and includes all inliers.

In this example, since all samples have roughly the same energy (ℓ_2 norm), we can propose a simple scheme for estimating the λ value in which the phase transition occurs. Specifically, we can compute the mean energy of all samples, namely $ME = \frac{1}{N} \sum_i^N \|\mathbf{x}_i\|_2^2$. Since we can not reliably reconstruct the outliers (based on our data model), we expect the error for reconstructing outliers to be $\sim ME$. Therefore, for any $\lambda > ME$, PRAE- ℓ_1 should include outliers since $\|\mathbf{x}_i - \hat{\mathbf{x}}_i\|_2^2$ is compared to λ in loss (see (5)). On the other hand, if $\lambda < ME$, PRAE- ℓ_1 should exclude outliers (based on the same argument). For PRAE- ℓ_0 , this argument is not precise; nonetheless, we observe that ME lines well with the phase transition of both models. This is presented as a dashed black line in Figure 3.

Another scheme to tune the regularization parameter is based on the reconstruction loss of unseen samples (a validation set). Here, we assume that inliers can be represented by a low dimensional space while outliers can not. By evaluating the model's reconstruction error on unseen samples, we can check if the model suffered from overfitting on anomalies or has used only inliers. We repeat the experiment above but evaluate the average reconstruction loss on 200 unseen sample generated from the same linear model with the same portion of outliers (25%). As evident in the bottom panel of Figure 3 both models lead to the smallest reconstruction loss for λ values that correspond to perfect F1-score. We observe that PRAE- ℓ_0 leads to a higher reconstruction error for large values of λ . This might indicate that the inclusion of all samples occurs earlier in training leading to stronger overfitting.

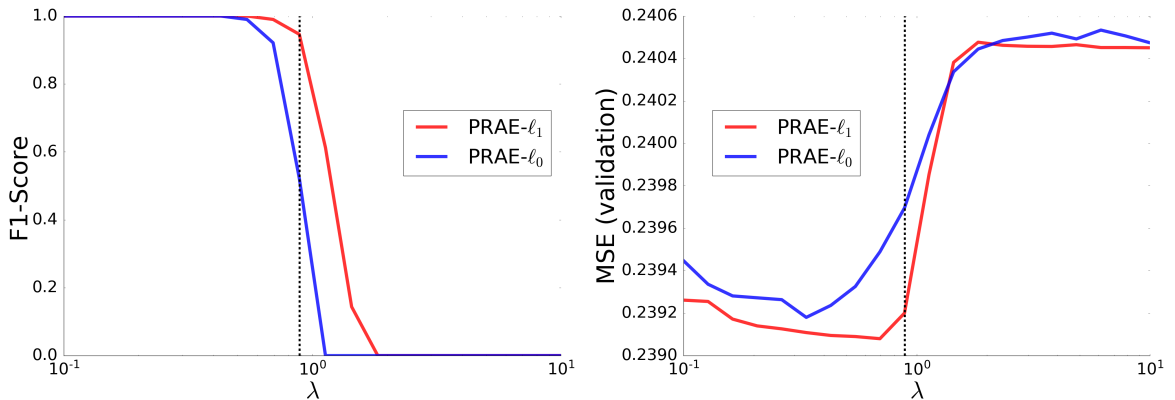


Figure 3: Phase transition of PRAE. As we increase λ above a certain threshold PRAE starts to include outliers resulting in lower F1-score (left panel) and larger reconstruction error (MSE) on unseen samples (right panel).

Table 1: Description of the real datasets used for evaluating the quality of outlier detection.

Data set	Samples	Features	Outliers(%)
Lympho	148	18	4.1
Ecoli	336	7	2.7
Cardio	1831	21	9.6
Yeast	1364	8	4.8
Musk	3062	166	3.1
Thyroid	3772	6	2.4
MNIST-S	5127	784	5.2
Pendigits	6870	16	2.2
Mammography	11183	6	2.3
Shuttle	49097	9	7.1

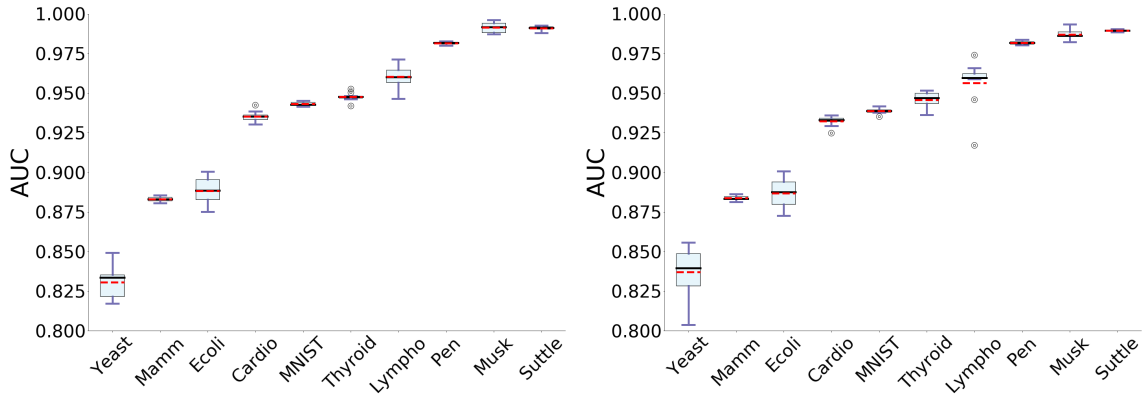


Figure 4: Box plots presenting the AUC of the proposed approach on several real datasets. The left and right panels represent PRAE- ℓ_0 and PRAE- ℓ_1 respectively. We use 10 different random initializations on each dataset and compute the AUC after convergence.

6.3 Real Data

Next, we evaluate the proposed approach on several real-world datasets from [39]. The properties of all datasets appear in table 1. Following [21, 40], we evaluate the quality of anomaly detection using Receiver Operating Characteristic (ROC) curves. The ROC measures the trade-off between true positive and false-positive rates. The true positive rate is defined as the ratio between identified anomalies and true anomalies. While the false positive rate is the portion of normal samples identified as anomalies. The ROC curves are summarized by measuring the AUC (area under the curve). We compare our method to several strong baselines with code available at [41]. Specifically, we use CBLOF [42] a local clustering-based approach, COF [43] which uses the density of the data, SOD [44] and HBOS [45] which are based on proximity, IForest [46] and LSCP [47] which are ensemble methods, and the probabilistic ABOD [48] scheme.

We train our proposed AE with an encoder-decoder pair with five hidden layers each of size 10; the hidden dimension is 1 (this might not be optimal but worked well across most datasets). We use the heuristic proposed in section 6.2 to tune the regularization parameter to $\lambda = 1 < ME$. The learning rate is 0.001, and the batch size is $\lceil N/50 \rceil$. We run all methods 10 times and record the ROC for each run. In table 2 we present the median AUC of the proposed method and all baselines. These results show that the proposed approach compares favorably to leading methods on a wide range of datasets. Specifically, PRAE outperform all baselines in

Data set	CBLOF	ABOD	COF	IForest	SOD	LSCP	HBOS	$\ell_{2,1}$ -AE	RandNet*	PRAE- ℓ_0	PRAE- ℓ_1
Thyroid	91.68	48.73	58.34	97.64	87.57	81.91	95.06	81.39	90.42	94.78	94.69
Cardio	85.31	49.87	51.79	92.15	69.19	59.42	88.14	88.10	92.87	94.28	93.87
Ecoli	87.90	75.72	87.77	86.41	82.67	86.71	81.44	44.21	85.42	88.94	89.09
Lympho	95.12	72.53	88.08	99.98	92.08	97.38	99.01	98.72	99.06	96.09	95.98
Pendigits	91.73	63.13	52.33	95.18	64.91	47.39	92.69	93.73	93.44	97.56	97.47
Yeast	68.63	56.81	53.18	79.30	61.79	61.62	78.98	70.58	82.95	83.37	83.95
Musk	95.17	68.04	52.31	97.46	89.93	60.45	98.91	98.96	NA	99.17	98.61
Mammography	81.42	83.00	71.18	86.62	77.51	50.53	83.00	81.31	NA	88.31	88.33
Shuttle	66.50	58.22	53.59	99.67	50.74	53.29	98.42	97.78	NA	99.13	98.95
MNIST-S	52.97	51.11	52.23	83.37	51.14	51.57	51.36	90.39	NA	93.54	93.31
Average-AUC	82.38	62.57	61.93	91.78	72.83	64.93	86.70	84.52	90.69	93.52	93.43
Median rank	6	9	9	3	7	8	4	5	NA	2	2

Table 2: Performance comparison with several leading anomaly detection baselines. We present the median AUC over 10 runs. *Results from the original paper are reported when available.

terms of average AUC. Moreover both PRAE- ℓ_0 and PRAE- ℓ_1 have a median rank of 2, and each would have a median rank 1 in the absence of the other approach as a competitor.

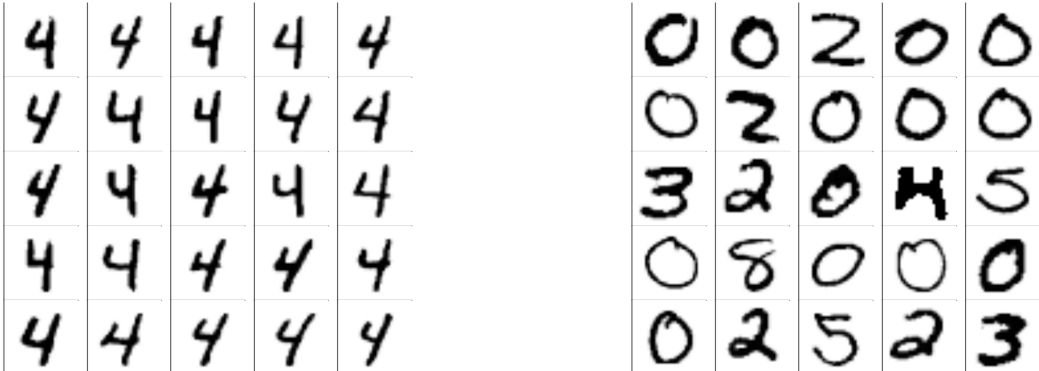


Figure 5: Left: 25 most inlaying images in the MNIST-S experiment. Right: 25 most outlying images in the MNIST-S experiment.

6.4 Small MNIST data set (MNIST-S)

In the next example, we follow the setting suggested in [22]. The authors proposed to use a subset of the MNIST handwritten dataset to evaluate anomaly detection capabilities. They construct the subset by mixing 4859 nominal instances of the digit '4' and adding 265 anomalies randomly sampled from all other digits. Following [22], We use a linear AE with one hidden layer of size 24. Evaluation of the AUC of our method compared to all baselines appears in Table 2. This example appears to be especially challenging for most baselines; we believe that this is due to the relatively high dimensionality of this data. In the top panel of Fig. 5, we present the 25 most *inlaying* images as identified by our method. In the bottom right panel of this figure, we present the 25 most *outlying* images as identified by the proposed approach. In this example, the identified inliers share a standard “simple” structure of the digit '4'. On the other hand, most identified outliers are indeed of different digits, except one example, which is somewhat of an unusual instance of the digit '4'.

7 Conclusion

In this work, we present a novel methodology for anomaly detection. Our method, which we call Probabilistic Robust autoencoder (PRAE), is based on a regularized AE designed to remove samples that do not lie near a low dimensional manifold. Specifically, we multiply each data instance with an approximately binary random variable and add a penalty term to the AE training to encourage sparsity of the number of samples used by the model. We prove an equivalent between the solution of our probabilistic formulation and the solution of an intractable ℓ_0 regularized AE. Finally, we demonstrate different properties of the proposed method using extensive simulations. Overall, we obtain several state-of-the-art results on challenging synthetic and real-world datasets.

References

- [1] Michael Lenning, Joseph Fortunato, Tai Le, Isaac Clark, Ang Sherpa, Soyeon Yi, Peter Hofsteen, Geethapriya Thamilarasu, Jingchun Yang, Xiaolei Xu, et al. Real-time monitoring and analysis of zebrafish electrocardiogram with anomaly detection. *Sensors*, 18(1):61, 2018.
- [2] Ofir Lindenbaum, Neta Rabin, Yuri Bregman, and Amir Averbuch. Multi-channel fusion for seismic event detection and classification. In *2016 IEEE International Conference on the Science of Electrical Engineering (ICSEE)*, pages 1–5. IEEE, 2016.
- [3] Y Bregman, O Lindenbaum, and N Rabin. Array based earthquakes-explosion discrimination using diffusion maps. *Pure and Applied Geophysics*, 178(7):2403–2418, 2021.
- [4] Ashima Chawla, Paul Jacob, Brian Lee, and Sheila Fallon. Bidirectional lstm autoencoder for sequence based anomaly detection in cyber security. *International Journal of Simulation-Systems, Science & Technology*, 2019.
- [5] Markus M Breunig, Hans-Peter Kriegel, Raymond T Ng, and Jörg Sander. Lof: identifying density-based local outliers. In *Proceedings of the 2000 ACM SIGMOD international conference on Management of data*, pages 93–104, 2000.
- [6] Wen Jin, Anthony KH Tung, and Jiawei Han. Mining top-n local outliers in large databases. In *Proceedings of the seventh ACM SIGKDD international conference on Knowledge discovery and data mining*, pages 293–298, 2001.
- [7] Jian Tang, Zhixiang Chen, Ada Wai-Chee Fu, and David W Cheung. Enhancing effectiveness of outlier detections for low density patterns. In *Pacific-Asia Conference on Knowledge Discovery and Data Mining*, pages 535–548. Springer, 2002.
- [8] Wen Jin, Anthony KH Tung, Jiawei Han, and Wei Wang. Ranking outliers using symmetric neighborhood relationship. In *Pacific-Asia conference on knowledge discovery and data mining*, pages 577–593. Springer, 2006.
- [9] Hans-Peter Kriegel, Peer Kröger, Erich Schubert, and Arthur Zimek. Loop: local outlier probabilities. In *Proceedings of the 18th ACM conference on Information and knowledge management*, pages 1649–1652, 2009.

[10] Valentino Constantinou. Pynomaly: Anomaly detection using local outlier probabilities (loop). *Journal of Open Source Software*, 3(30):845, 2018.

[11] Yariv Aizenbud, Amit Bermanis, and Amir Averbuch. Pca-based out-of-sample extension for dimensionality reduction. *arXiv preprint arXiv:1511.00831*, 2015.

[12] Sridhar Ramaswamy, Rajeev Rastogi, and Kyuseok Shim. Efficient algorithms for mining outliers from large data sets. In *Proceedings of the 2000 ACM SIGMOD international conference on Management of data*, pages 427–438, 2000.

[13] Fabrizio Angiulli and Clara Pizzuti. Fast outlier detection in high dimensional spaces. In *European conference on principles of data mining and knowledge discovery*, pages 15–27. Springer, 2002.

[14] Amol Ghosh, Srinivasan Parthasarathy, and Matthew Eric Otey. Fast mining of distance-based outliers in high-dimensional datasets. *Data Mining and Knowledge Discovery*, 16(3):349–364, 2008.

[15] Yariv Aizenbud and Barak Sober. Non-parametric estimation of manifolds from noisy data. *arXiv preprint arXiv:2105.04754*, 2021.

[16] Sam T Roweis and Lawrence K Saul. Nonlinear dimensionality reduction by locally linear embedding. *Science*, 290(5500):2323–2326, 2000.

[17] Erez Peterfreund, Ofir Lindenbaum, Felix Dietrich, Tom Bertalan, Matan Gavish, Ioannis G Kevrekidis, and Ronald R Coifman. Local conformal autoencoder for standardized data coordinates. *Proceedings of the National Academy of Sciences*, 117(49):30918–30927, 2020.

[18] Karl Pearson. LIII. on lines and planes of closest fit to systems of points in space. *The London, Edinburgh, and Dublin Philosophical Magazine and Journal of Science*, 2(11):559–572, 1901.

[19] Yann LeCun et al. Generalization and network design strategies. *Connectionism in perspective*, 19:143–155, 1989.

[20] Gilad Lerman and Tyler Maunu. An overview of robust subspace recovery. *Proceedings of the IEEE*, 106(8):1380–1410, 2018.

[21] Jinghui Chen, Saket Sathe, Charu Aggarwal, and Deepak Turaga. Outlier detection with autoencoder ensembles. In *Proceedings of the 2017 SIAM international conference on data mining*, pages 90–98. SIAM, 2017.

[22] Chong Zhou and Randy C Paffenroth. Anomaly detection with robust deep autoencoders. In *Proceedings of the 23rd ACM SIGKDD International Conference on Knowledge Discovery and Data Mining*, pages 665–674, 2017.

[23] Yezheng Liu, Zhe Li, Chong Zhou, Yuanchun Jiang, Jianshan Sun, Meng Wang, and Xiangnan He. Generative adversarial active learning for unsupervised outlier detection. *IEEE Transactions on Knowledge and Data Engineering*, 32(8):1517–1528, 2019.

[24] Dan Hendrycks, Mantas Mazeika, and Thomas Dietterich. Deep anomaly detection with outlier exposure. *arXiv preprint arXiv:1812.04606*, 2018.

[25] Siqi Wang, Yijie Zeng, Xinwang Liu, En Zhu, Jianping Yin, Chuanfu Xu, and Marius Kloft. Effective end-to-end unsupervised outlier detection via inlier priority of discriminative network. In *NeurIPS*, pages 5960–5973, 2019.

[26] Elad Plaut. From principal subspaces to principal components with linear autoencoders. *arXiv preprint arXiv:1804.10253*, 2018.

[27] Yutaro Yamada, Ofir Lindenbaum, Sahand Negahban, and Yuval Kluger. Feature selection using stochastic gates. In *International Conference on Machine Learning*, pages 10648–10659. PMLR, 2020.

[28] Ofir Lindenbaum, Moshe Salhov, Amir Averbuch, and Yuval Kluger. Deep gated canonical correlation analysis. *arXiv preprint arXiv:2010.05620*, 2020.

[29] Ofir Lindenbaum, Uri Shaham, Jonathan Svirsky, Erez Peterfreund, and Yuval Kluger. Differentiable unsupervised feature selection based on a gated laplacian. *Neural Information Processing Systems (NeurIPS)*, 2021.

[30] Ofir Lindenbaum, Moshe Salhov, Amir Averbuch, and Yuval Kluger. ell_0 -based sparse canonical correlation analysis. *arXiv preprint arXiv:2010.05620*, 2020.

[31] Soham Jana, Henry Li, Yutaro Yamada, and Ofir Lindenbaum. Support recovery with stochastic gates: Theory and application for linear models. *arXiv preprint arXiv:2110.15960*, 2021.

[32] Mayu Sakurada and Takehisa Yairi. Anomaly detection using autoencoders with nonlinear dimensionality reduction. In *Proceedings of the MLSDA 2014 2nd workshop on machine learning for sensory data analysis*, pages 4–11, 2014.

[33] Stephen Boyd, Stephen P Boyd, and Lieven Vandenberghe. *Convex optimization*. Cambridge university press, 2004.

[34] Gilad Lerman and Tyler Maunu. Fast, robust and non-convex subspace recovery. *Information and Inference: A Journal of the IMA*, 7(2):277–336, 2018.

[35] Teng Zhang. Robust subspace recovery by tyler’s m-estimator. *Information and Inference: A Journal of the IMA*, 5(1):1–21, 2016.

[36] Gilad Lerman, Michael B McCoy, Joel A Tropp, and Teng Zhang. Robust computation of linear models by convex relaxation. *Foundations of Computational Mathematics*, 15(2):363–410, 2015.

[37] Zhouchen Lin, Minming Chen, and Yi Ma. The augmented lagrange multiplier method for exact recovery of corrupted low-rank matrices. *arXiv preprint arXiv:1009.5055*, 2010.

[38] Tyler Maunu, Teng Zhang, and Gilad Lerman. A well-tempered landscape for non-convex robust subspace recovery. *Journal of Machine Learning Research*, 20(37), 2019.

[39] Rayana Shebuti. ODDS library, 2016.

[40] Yoshinao Ishii and Masaki Takanashi. Low-cost unsupervised outlier detection by autoencoders with robust estimation. *Journal of Information Processing*, 27:335–339, 2019.

- [41] Yue Zhao, Zain Nasrullah, and Zheng Li. Pyod: A python toolbox for scalable outlier detection. *Journal of Machine Learning Research*, 20(96):1–7, 2019.
- [42] Zengyou He, Xiaofei Xu, and Shengchun Deng. Discovering cluster-based local outliers. *Pattern Recognition Letters*, 24(9-10):1641–1650, 2003.
- [43] Jian Tang, Zhixiang Chen, Ada Wai-Chee Fu, and David W Cheung. Enhancing effectiveness of outlier detections for low density patterns. In *Pacific-Asia Conference on Knowledge Discovery and Data Mining*, pages 535–548. Springer, 2002.
- [44] Hans-Peter Kriegel, Peer Kröger, Erich Schubert, and Arthur Zimek. Outlier detection in axis-parallel subspaces of high dimensional data. In *Pacific-Asia Conference on Knowledge Discovery and Data Mining*, pages 831–838. Springer, 2009.
- [45] Markus Goldstein and Andreas Dengel. Histogram-based outlier score (hbos): A fast unsupervised anomaly detection algorithm. *KI-2012: Poster and Demo Track*, pages 59–63, 2012.
- [46] Fei Tony Liu, Kai Ming Ting, and Zhi-Hua Zhou. Isolation forest. In *2008 Eighth IEEE International Conference on Data Mining*, pages 413–422. IEEE, 2008.
- [47] Yue Zhao, Zain Nasrullah, Maciej K Hryniwicki, and Zheng Li. Lscp: Locally selective combination in parallel outlier ensembles. In *Proceedings of the 2019 SIAM International Conference on Data Mining*, pages 585–593. SIAM, 2019.
- [48] Hans-Peter Kriegel, Matthias Schubert, and Arthur Zimek. Angle-based outlier detection in high-dimensional data. In *Proceedings of the 14th ACM SIGKDD international conference on Knowledge discovery and data mining*, pages 444–452, 2008.